



Modeling Soot Oxidation and Gasification with Bayesian Statistics

Alexander J. Josephson,[†] Neal D. Gaffin,[†] Sean T. Smith,[‡] Thomas H. Fletcher,[†] 
and David O. Lignell^{*,†} 

[†]Department of Chemical Engineering, Brigham Young University, Provo, Utah 84602, United States

[‡]Department of Chemical Engineering, University of Utah, Salt Lake City, Utah 84112, United States

Supporting Information

ABSTRACT: This paper presents a statistical method for model calibration using data collected from literature. The method is used to calibrate parameters for global models of soot consumption in combustion systems. This consumption is broken into two different submodels: first for oxidation where soot particles are attacked by certain oxidizing agents; second for gasification where soot particles are attacked by H₂O or CO₂ molecules. Rate data were collected from 19 studies in the literature and evaluated using Bayesian statistics to calibrate the model parameters. Bayesian statistics are valued in their ability to quantify uncertainty in modeling. The calibrated consumption model with quantified uncertainty is presented here along with a discussion of associated implications. The oxidation results are found to be consistent with previous studies. Significant variation is found in the CO₂ gasification rates.

1. INTRODUCTION

Modeling of soot formation in combustion systems has been an extensive area of research over the last several decades. The emission of particulate matter in combustion processes has proven to be a significant health concern since these particles can be taken-up by cells in the lung. Through this absorption, these particles enter the circulatory system and can lodge in organs such as the liver, heart, and kidneys, leading to reduced or altered organ function.^{1,2} In addition, soot emissions have become an increasing concern in the environment affecting cloud formation and climate change.^{3,4} Within a given combustion process, the presence of soot can have a significant impact on radiative heat fluxes⁵ and hence flame temperature and pollutant formation.

Given these impacts of soot, extensive studies concerning the formation and evolution of soot in combustion processes have been performed, for example, see refs 6 and 7 and references therein. From these studies, researchers commonly define the formation of soot to take place in five stages: nucleation, coagulation, growth, aggregation, and oxidation. Four of these stages involve the formation and evolution of soot, but only one, oxidation, deals with the consumption of the soot once it forms.⁸ Some of the first investigators of soot oxidation assumed that soot was consumed solely via reaction of an O₂ molecule with the particle surface,⁹ and oxidation models were developed based on the O₂ concentration. It was quickly determined that the presence of OH molecules greatly influenced rates of soot consumption and hence it was included in oxidation models.¹⁰ In more recent studies, emphasis has been placed on the influence of O radicals in flames,¹¹ particularly in high temperature flames where the O radical concentration is relatively high.¹² However, due to the coexistence of O with O₂ and OH, it is difficult to experimentally differentiate between oxidation via O versus oxidation by O₂ and OH without molecular modeling. As a

result, many models do not explicitly consider oxidation by O; rather this effect is implicit in the rates used for O₂ or OH.

In recent years, there has been an increased interest in oxygen-enriched combustion (oxy-fuel combustion) as a means of enabling carbon capture.^{13,14} Oxy-fuel combustion often involves higher temperatures and higher H₂O and CO₂ concentrations due to flue gas recycling. Most soot models have historically ignored gasification reactions, which tend to be small compared to oxidation reactions in common combustion systems.¹⁵ However, this may not be true in oxy-fuel combustion, where the higher H₂O and CO₂ concentrations interact with particle surfaces and lead to increased soot consumption.¹⁶

Current research on soot consumption has placed large emphasis on the evolution of particle surface reactivity. Researchers have developed mechanisms reflecting the many elementary chemical reactions^{17,18} and mechanical changes¹⁹ occurring at the particle surface during consumption. There is also ongoing research investigating correlations between particle surface reactivity and the particle inception environment.^{20,21}

Many experiments have been performed to investigate soot oxidation in premixed and non-premixed flames. Fewer studies have been performed of soot gasification. In this paper, we analyze data from 19 experiments to develop soot oxidation and gasification models to predict soot consumption behavior over wide ranges of temperature and composition. To do this, we use Bayesian statistics to fit reaction model parameters to specified model forms. The methods presented, however, are general, and one purpose of this study is to illustrate the Bayesian method used. This method then allows the model to be easily extended to account for additional data sets, varying

Received: March 30, 2017

Revised: August 3, 2017

Published: August 22, 2017



model forms, or more generic problems. In addition to the presentation of the model and Bayesian method, all data sets and codes are made available as [Supporting Information](#).

The remainder of the paper is organized as follows. [Section 2](#) provides model forms and background information on the data sets used in the analysis, followed by a description of the Bayesian method used. [Section 3](#) presents results including model parameters and uncertainties. Finally, discussion and conclusions are presented in [sections 4 and 5](#), respectively.

2. METHODS

This section describes the oxidation and gasification models, the data sets used, and the Bayesian statistical model.

2.1. Oxidation Model. Although the process of soot oxidation is complicated, this study uses data collected from experiments over the last several decades to fit a simple global model for use in simulation. This model is based on irreversible global oxidation reactions including the following:



This global model is both computationally inexpensive and simple but still reasonably accurate. This model is designed for use in large-scale simulations sensitive to computational cost. As this consumption model will only require basic information for evaluation (local temperature, species concentrations, and particle size), it reduces the number of transported and computed terms, which can be costly in large-scale simulations.

This model is not a complete mechanism for soot oxidation and should be used with caution when considered for simulations outside of flames and may not be appropriate for detailed simulations with fully resolved physics. A full mechanism for soot oxidation may contain hundreds of possible reactions as soot particles react with various oxidizing species.²² Since these reactions occur at the particle surface, considerations for gaseous species concentrations, mass transport, and surface chemistry would all need to be included.

Due to the relatively small size of soot particles, soot oxidation models usually assume particles are in the free molecular regime and transport limitations of oxidizing molecules to the particle surface are ignored. Transport effects may, however, become important for large soot aggregates, especially in systems such as coal combustion, for which relatively high soot concentrations may be expected. Besides external transport, a complete mechanism would need to consider particle surface and internal structure properties, such as porosity, in a manner similar to char oxidation models.²³ Internal transport of O_2 during soot oxidation has also been studied recently.^{24,25}

As the soot particle oxidizes, the surface chemistry changes and further affects later oxidation reactions.²⁶ When oxidation first begins, aliphatic branches first react with oxidizing agents due to the weaker bonds holding these atoms to the particle surface. Once these branches are all consumed, aromatic structures begin to break up, and depending on the size of the aromatic cluster, will have varying activation energies. This means that the oxidation consumption reactions are not uniform throughout the process of consumption but will likely vary in rate as the particle surface chemistry changes. This level of detail, while important to note, is not normally considered in soot modeling and is not used in the models presented here.

The following simple global model is proposed:

$$r_{\text{ox}} = \frac{1}{T^{0.5}} \left(A_{\text{O}_2} P_{\text{O}_2} \exp\left[\frac{-E_{\text{O}_2}}{RT}\right] + A_{\text{OH}} P_{\text{OH}} \right) \quad (3)$$

Here, r_{ox} ($\text{kg}_{\text{soot}} \text{m}_{\text{soot}}^{-2} \text{s}^{-1}$) denotes the oxidation rate, T is temperature, A is an Arrhenius pre-exponential factor, P is partial pressure, R is the gas constant, and E is an activation energy. This global model is a modified Arrhenius equation with dependence on temperature and concentrations of O_2 and OH . Similar in form to

previously developed models,²⁷ it contains three fitted parameters: A_{O_2} , E_{O_2} , and A_{OH} . [Equation 3](#) assumes the following:

- 1. Oxidizing Agents.** Oxidation is assumed to occur by O_2 and OH only. This is adequate for the majority of flames. In flames, it was found that the OH and O account for most of the consumption of soot,¹¹ while in the TGA experiments nearly all consumption is attributed to O_2 and O .²⁸ In turbulent flames, higher mixing rates may allow for greater interaction between O_2 and soot than is found in laminar flames. As noted above, O rates are taken as implicit scales with OH rates in flames and O_2 rates in TGA experiments, and so O oxidation is not explicitly considered here.
- 2. Transport.** Surface concentrations of oxidizing species are taken as the local concentrations in the surrounding environment. Any transport effects are then implicit in the pre-exponential factor for the rate expressions.
- 3. Surface Chemistry.** This model assumes that the surface chemistry of the particle is uniform and constant in time. Conversion-dependent changes in rate coefficients are approximated with an effective activation energy. This effective activation energy is what is used for the O_2 reaction, while the effective activation energy for the OH reaction is considered to be negligibly small because OH is such an effective oxidizer.²⁷

2.2. Oxidation Data. Experiments measuring soot oxidation have been carried out in many forms, and the literature contains many different studies. In this work, data were taken from 13 different sources and typically fall under two different types of studies: those soot experiments performed with flames and those in a nonflame environment. Most of the flame environments use a laminar flame; the nonflame experiments mostly took place through thermogravimetric analysis (TGA), where soot particles were exposed to an oxidized environment at elevated temperatures. [Table 1](#) summarizes the different experiments used for this study including the experimental method and the number of data points.

Each of these experiments was performed differently, and results were presented in different ways. As experimental uncertainties were not reported in the literature, a full analysis considering both model and experimental uncertainties is not presented here. We have no reason to believe that the published experimental data that we chose for this study is unreliable, though certainly all measurements have error, and the magnitude of such errors may vary among the experiments. Quantified experimental errors would improve the results presented in terms of the credible intervals (the Bayesian analog of confidence intervals) and aid in ascribing variability to data and model forms. All data needed to be converted to a common format for use in the proposed model. This conversion of data, referred to as the instrumental model, involved making some assumptions about the data or experimental conditions, thus introducing additional uncertainty. The instrument model extracted a rate (measured in $\text{kg m}^{-2} \text{s}^{-1}$), temperature (K), and species partial pressures (Pa) from each data set to be used in the Bayesian analysis. A brief description of the experiments along with some aspects of the instrumental model used are discussed below.

Fenimore and Jones²⁹ created soot with a fuel-rich ethylene premixed flame, and the soot was then fed to a second burner fired with a fuel-lean premixed flame. Oxidation rates were taken from this second flame using quench probe measurements. Local gas temperatures were reported and used to find local species concentrations assuming an equilibrium state of the GRI 3.0 mechanism in Cantera, a suite of object-oriented software tools for problems involving chemical kinetics, thermodynamics, and transport processes.³⁸

Kim et al.,^{31,32} Neoh et al.,³⁰ and Xu et al.,³⁴ all measured oxidation rates in laminar diffusion flames. Local temperatures and concentrations of oxidizing agents were reported along the flame. Rates were measured and converted to collision efficiencies for the different oxidizing species, and these efficiencies were reported. For our study, these collision efficiencies were converted back to rates through the following equation:

Table 1. Studies from Which Oxidation Data Were Extracted for Model Development

study	data points	oxidizing agent	experiment	temp (K)
Fenimore and Jones, 1967 ²⁹	3	O ₂ and OH	premixed ethylene flame	1530–1710
Neoh et al., 1981 ³⁰	14	O ₂ and OH	laminar methane diffusion flame	1768–1850
Ghiassi et al., 2016 ¹⁷	54	O ₂ and OH	premixed varied-fuel flame	1265–1570
Kim et al., 2004 ³¹	2	O ₂ and OH	laminar ethylene diffusion flame	1735–1740
Kim et al., 2008 ³²	3	O ₂ and OH	laminar ethylene diffusion flame	1892–1916
Garo et al., 1990 ²²	6	O ₂ and OH	laminar methane diffusion flame	1809–1851
Puri et al., 1994 ³³	15	O ₂ and OH	laminar methane diffusion flame	1236–1774
Xu et al., 2003 ³⁴	15	O ₂ and OH	laminar mixed hydrocarbon diffusion flames	1775–1900
Lee et al., 1962 ⁹	29	O ₂ and OH	laminar mixed hydrocarbon diffusion flame	1315–1660
Chan et al., 1987 ³⁵	14	O ₂	TGA	780–1210
Higgins et al., 2002 ³⁶	28	O ₂	tandem differential mobility analyzer	773–1348
Kalogirou and Samaras, 2010 ²⁸	6	O ₂	TGA	823–973
Sharma et al., 2012 ³⁷	18	O ₂	TGA	823–923

$$r_{\text{ox}} = \frac{\eta_i m_{\text{cr},i} C_i \bar{v}}{4} \quad (4)$$

where η_i is the collision efficiency of species i , $m_{\text{cr},i}$ is the mass of carbon removed due to the oxidation by species i per mole of species i , C_i is the molar concentration of species i , and \bar{v} is the mean molecular velocity. Data from each of these experiments are assumed to be independent and were all used to calibrate the Arrhenius pre-exponential factors and effective activation energies in eq 3 using Bayesian statistics.

Ghiassi et al.¹⁷ used a two stage burner where a liquid fuel mixture was injected into a premixed-fuel-rich region where soot particles were formed and then passed into a second fuel-lean region where oxidation occurred. Particles were collected in the second region and analyzed using a scanning mobility particle sizer. Rates of oxidation were extracted from the change in particle size distribution in the fuel-lean region. Local temperatures and O₂ concentrations were measured, while OH concentrations were modeled and reported by the experimenters.

Garo et al.²² and Puri et al.³³ both measured oxidation rates of soot using laser-induced fluorescence in a methane–air laminar diffusion flame. Temperatures, species partial pressures, and oxidation rates were all reported. Reported values of O₂ and OH were not used. Instead the calculated equilibrium values were used to preserve consistency between these data and other collected data. Reported rate values were converted to units of kg m⁻² s⁻¹ for evaluation.

Chan et al.³⁵ and Lee et al.⁹ each measured oxidation rates using a quench probe in laminar diffusion flames burning propane and natural gas, respectively. Chan et al. performed additional experiments using a TGA technique. For the flame, local gas temperatures were reported along with oxidation rates. Those temperatures were used to find local concentrations of O₂ and OH along the flame front (stoichiometric point), assuming an equilibrium state of the GRI 3.0 mechanism in Cantera. The TGA temperature and rates were also reported along with a partial pressure of O₂ in the experimental setup. The reported rate values were converted to units of kg m⁻² s⁻¹ for evaluation.

Higgins et al.³⁶ used a tandem differential mobility analyzer technique in which monodispersed particles, collected from an ethylene diffusion flame, were subjected to an elevated temperature in air and the change in particle diameter was measured. Particle diameter, temperature, and residence time were reported. Rates were extracted by the experimenters from these data by the following equation:

$$r_{\text{ox}} = \frac{\rho_s (d_1 - d_2)}{2t} \quad (5)$$

where the density of the soot particles (ρ_s) was assumed to be 1850 kg m³. The above equation reflects the change of mass per surface area over a residence time during which the soot particle was exposed to oxidizer. Partial pressures were again calculated using equilibrium of the GRI 3.0 mechanism.

Kalogirou and Samaras²⁸ and Sharma et al.³⁷ both used TGA techniques to record oxidation rates of soot collected from a diesel engine. Reported data were temperature, O₂ concentrations, and calculated rate constant (k) values of a single-step Arrhenius equation:

$$r_{\text{ox,rep}} = k X_{\text{O}_2}^n \quad (6)$$

Kalogirou assumed a 0.75 order dependence of O₂, while Sharma assumed a 1.0 order dependence and used the partial pressure of O₂ rather than the molar fraction as displayed above. In both cases, the Arrhenius equation gave rate data in units of s⁻¹. These rates were converted to our desired rates by

$$r_{\text{ox}} = \frac{r_{\text{ox,rep}} \rho_s d_1}{6} \quad (7)$$

where the soot density was again assumed to be 1850 kg m³ and the initial particle diameter was assumed to be 50 nm.^{18,27} This equation is a reflection of the mass of soot consumed per unit of particle surface area.

2.3. Gasification Model. Gasification differs significantly from oxidation. Gasification generally has an endothermic heat of reaction, and most products are only partially oxidized. Examples of global gasification reactions include



and these are the reactions used in this work. As with oxidation reactions, these global reactions are considered irreversible. In the rate models presented below, the global nature of these reactions is reflected in nonunity reaction orders. Triatomic species are particularly important in gasification due to large amounts of potential energy contained within bond vibrations and rotations.¹⁴ Sometimes the collision of these molecules with a soot particle results in the transfer of enough energy to break bonds within the soot particle, similar to thermal pyrolysis. As a result of these collisions and reactions, gasification tends to produce a larger variety of product species than oxidation. Products of oxidation are usually limited to CO, CO₂, and H₂O. Gasification reactions, on the other hand, will often include these species along with H₂, small hydrocarbons, alcohols, carbonyls, and other species as products.³⁹

In oxy-fuel systems, the increased concentrations of CO₂ and H₂O are of interest. CO₂ is the most commonly considered gasification agent. H₂O is often considered to be an oxidizer; however, data in the literature has shown that the products of soot/H₂O reactions are more indicative of gasification than oxidation.³⁹ Other species are able to gasify as well, such as NO₂, and some research has been done on these reactions and rates.^{10,40}

Like oxidation, gasification tends to be a complex surface reaction, dependent on many of the same variables discussed above: transport effects, surface chemistry, and various gasification agents.⁴¹ As stated previously, gasification occurs via surface reactions with many different possible species, especially high-internal-energy molecules with energy to transfer upon collision. The model developed in this study only considers gasification by CO₂ and H₂O since these two species are

thought to be the only gasifying agents in high enough concentrations to have a notable effect in either air-fired or oxy-fired boiler environments.

Although soot consumption via oxidation has long been an area of research, gasification of soot has been much less studied. While gasification has long been discussed as a possible method for removing soot build-up on filters in diesel engines, relatively little experimentation has been done and gasification rates are not well-known. In recent years, there has been increased interest in solid-fuel gasification for use in combined turbine cycles. During this gasification process soot has the potential to form, and researchers have begun exploring soot models for these systems. Due to the absence of oxygen in these systems, the only source of soot consumption is gasification. As a result, there have been a few recent studies that consider gasification of soot, particularly biomass-derived soots. These experiments, along with a few others found in the literature, are used to form the proposed model of this study.

This model consists of two additive rate terms for gasification by CO_2 and H_2O :

$$r_{\text{gs}} = r_{\text{CO}_2} + r_{\text{H}_2\text{O}} \quad (10)$$

$$r_{\text{CO}_2} = A_{\text{CO}_2} P_{\text{CO}_2}^{0.5} T^2 \exp\left(\frac{-E_{\text{CO}_2}}{RT}\right) \quad (11)$$

$$r_{\text{H}_2\text{O}} = \frac{A_{\text{H}_2\text{O}} P_{\text{H}_2\text{O}}^n}{T^{1/2}} \exp\left(\frac{-E_{\text{H}_2\text{O}}}{RT}\right) \quad (12)$$

Rates in these equations are defined in units of ($\text{kg}_{\text{soot}} \text{m}_{\text{soot}}^{-2} \text{s}^{-1}$). Equation 11 represents gasification due to attack by CO_2 with a modified Arrhenius equation dependent on temperature and the partial pressure of CO_2 . The CO_2 order of reaction was extracted from ref 26. The temperature dependence order was set after a series of statistical fittings to limit the number of adjustable parameters. Equation 11 contains two adjustable parameters: the Arrhenius pre-exponential factor and activation energy, that are fit empirically to data with Bayesian statistics, as described below.

Equation 12 represents gasification by H_2O . Like eq 11, eq 12 also contains temperature and partial pressure dependencies, two similar adjustable parameters, and a third adjustable parameter, n , for the H_2O order of reaction. These two equations are analyzed separately because researchers have studied gasification by CO_2 and H_2O independently.

2.4. Gasification Data. Table 2 summarizes the gasification data used here. The data are limited but represent the experimentation

Table 2. Studies from Which Gasification Data Were Extracted for Model Development

study	no. of data points	gasifying agent	temp (K)
Abian et al., 2012 ¹⁶	14	CO_2	1132–1650
Kajitani et al., 2010 ²⁶	6	CO_2	1123–1223
Qin et al., 2013 ²⁰	3	CO_2	305–1261
Otto et al., 1980 ⁴²	2	H_2O and CO_2	1066–1160
Arnal et al., 2012 ⁴³	6	H_2O	1273
Chhiti et al., 2013 ⁴⁴	28	H_2O	1373–1673
Neoh et al., 1981 ³⁰	14	H_2O	1777–1815
Xu et al., 2003 ³⁴	15	H_2O	1770–1840

done with regard to soot gasification found in the literature. More data are desirable to obtain a more robust model, and one purpose of this study is to present a method that can easily incorporate additional data as they become available.

Like the oxidation experiments, each of the gasification experiments was performed differently, and results were presented in various ways. As for the oxidation experiments, uncertainties for gasification were not included in the literature; however they are believed to be larger than the uncertainties found in the oxidation experiments since the magnitude of gasification rates are smaller than those for oxidation and

thus small measurement errors yield higher relative errors. These larger uncertainties are reflected in larger uncertainties in the model as well. In order to use these data in the proposed model, each data point had to be converted to an instrumental model. The following is a brief description of each experiment along with some aspects of the instrumental model used.

Abian et al.¹⁶ produced soot particles in an ethylene diffusion flame. These particles were collected and placed in a TGA under a N_2/CO_2 environment. The partial pressure of CO_2 was set, and temperature was calculated given the elapsed time and a constant heating rate. Rates of consumption were measured as the particles were heated, and these rates were reported as a conversion of the original mass over time. This reported rate was converted to $\text{kg m}^{-2} \text{s}^{-1}$ using the original sample mass along with an assumed initial particle diameter of 50 nm. Soot samples were prepared under different environments by varying feed rates into the original ethylene diffusion flame; however, it was found that the gasification rate minimally depended on the environment in which the soot was produced. For the purposes of this model, that dependence was accounted for by taking an average rate across all samples collected in different environments.

Kajitani et al.²⁶ and Qin et al.²⁰ also used a TGA to measure the reactivity of soot collected from biomass derived soots. Both reported partial pressures of CO_2 within the TGA as well as conversion of soot particles as the experiment progressed. Rates were extracted using the given particle heating rates along with an assumed initial particle diameter of 50 nm. Of particular note is the observation made by Qin et al. that soot particles have a significant difference in reactivity compared to char particles. Kajitani et al. remarked that the surface chemistry of soot seemed to change throughout the experiment but minimally affected rates of gasification.

Otto et al.⁴² were the first to experiment on soot gasification by collecting diesel soot on filters and exposing that soot to exhaust gas from four CVS-CH cycles. TGA experiments were carried out first with H_2O as the gasifying agent and then repeated with CO_2 . Rates ($\mu\text{g m}^{-2} \text{s}^{-1}$), partial pressures of the gasifying agents, and temperatures were reported. Otto et al. noted that data collected for CO_2 gasification should be used with caution due to low accuracy.

Arnal et al.⁴³ used a flow reactor to study the water vapor reactivity of Printex-U, a commercial carbon black considered as a surrogate for diesel soot. Temperatures and the changing concentrations of CO , CO_2 , and H_2 were reported. Assuming the only source of carbon in the system came from the Printex-U, we determined a rate of soot consumption as the CO and CO_2 concentrations increased. Once again an initial particle diameter of 50 nm was assumed.

Chhiti et al.⁴⁴ explored soot gasification by H_2O in bio-oil gasification using a lab-scale Entrained Flow Reactor and reported the soot yield and temperature over time. Soot particles were added to the reactor and first pyrolyzed in an inert environment over a given amount of time. This was repeated in an environment containing a reported partial pressure of H_2O . The gasification rate was determined assuming a constant number of particles that lost mass uniformly from all particles.

The experiments of Neoh et al.³⁰ and Xu et al.³⁴ included H_2O reactions, and these were described in the previous section.

Data from each of these experiments are assumed to be independent and are all used to calibrate the parameters in the gasification model, eqs 10–12. Raw data extracted from experiments both in oxidation and on gasification, along with details of the conversions to instrumental models, can be found in the [Supporting Information](#).

2.5. Bayesian Statistics. The following section describes details of the Bayesian technique used to calibrate the model parameters. We recognize that this is a new-enough approach to be unfamiliar to many readers. Further details on the philosophical underpinnings of Bayesian inference are provided by Jaynes and Bretthorst.⁴⁵ A practical introduction to the basic methodologies of Bayesian inference is given by Gelman.⁴⁶

A brief introduction is provided here. Bayes' law is given by

$$f_{X|Y}(\mathbf{x}|y) \propto f_{Y|X}(y|\mathbf{x})f_X(\mathbf{x}) \quad (13)$$

We take \mathbf{x} to be the vector of model parameters and \mathbf{y} to be the vector of experimental data values; f denotes a probability density function (PDF). In words, Bayes' law states that the probability of getting a set of parameters given the data is proportional to the probability of getting the data given a set of parameters times the probability of getting the parameters. (The proportionality is used to imply that, as a PDF, f should be normalized so that it integrates to one.) The term on the left is called the posterior, and this is our objective. The value of \mathbf{x} where $f_{X|Y}$ is maximum is the mode and is the most probable set of model parameters (which are elements of vector \mathbf{x}) for the given data. The term $f_{Y|X}(\mathbf{y}|\mathbf{x})$ is called the likelihood, and $f_X(\mathbf{x})$ is called the prior. The three terms are described in more detail below. Bayes' law can be thought of as an inverse probability law: we evaluate the desired probability for \mathbf{x} given \mathbf{y} in terms of its inverse, the probability of \mathbf{y} given \mathbf{x} , along with the prior probability $f_X(\mathbf{x})$.

2.5.1. Likelihood. The likelihood function, $f_{Y|X}(\mathbf{y}|\mathbf{x})$ represents the probability of the data \mathbf{y} given a set of model parameters \mathbf{x} . This is evaluated as follows. Recall the data are a superset from multiple experiments, each providing multiple observations. As such, an individual data point is notated using two subscripts, $y_{z,i}$, the first indicating which experiment ($z = 1, 2, \dots, n_e$) and the second indicating the sample data point within that experiment ($i = 1, 2, \dots, n_{z,i}$). A given data point $y_{z,i}$ can be compared to the corresponding model value $\mu_{z,i}(\mathbf{x})$ for a given set of model parameters \mathbf{x} . We assume unbiased and independent (but identically distributed) observations within a single experiment and complete pairwise independence of observations between any two experiments. This allows the likelihood to be written as

$$f_{Y|X}(\mathbf{y}|\mathbf{x}) = \prod_{z=1}^{n_e} \prod_{i=1}^{n_{z,i}} p(y_{z,i}|\mu_{z,i}(\mathbf{x})) \quad (14)$$

where $p(y_{z,i}|\mu_{z,i}(\mathbf{x}))$ is the probability of an observation $y_{z,i}$ given the corresponding modeled point $\mu_{z,i}(\mathbf{x})$ evaluated with a set of parameters \mathbf{x} . The modeled point $\mu_{z,i}(\mathbf{x})$ (a soot consumption rate) is evaluated using one of eqs 3, 11, or 12. Each evaluation of $\mu_{z,i}(\mathbf{x})$ is performed using the state properties (temperature, species partial pressure) that correspond to the data point $y_{z,i}$.

When experimental uncertainty has been quantified, one can calculate the likelihood function in terms of the quantified uncertainty. However, should experimental uncertainty not be defined (as is the case here), we can evaluate the likelihood using a Gaussian form:

$$p(y_{z,i}|\mu_{z,i}(\mathbf{x})) = \frac{1}{\sqrt{2\pi\sigma_z^2}} \exp\left(-\frac{(y_{z,i} - \mu_{z,i}(\mathbf{x}))^2}{2\sigma_z^2}\right) \quad (15)$$

Each Gaussian function is centered on the parameter $\mu_{z,i}(\mathbf{x})$. Hence, the probability of the data given the model (the likelihood) is highest when the data $y_{z,i}$ and the modeled data $\mu_{z,i}$ coincide. The use of the Gaussian has introduced a new parameter, σ_z , which can be different for each experiment. σ_z is a scale parameter for a given experiment, and the set of σ_z is denoted by vector $\boldsymbol{\sigma}$. These parameters are computed as part of the solution, and as such, we augment the set of model parameters \mathbf{x} by including $\boldsymbol{\sigma}$ and denote this \mathbf{x}^* . That is, \mathbf{x}^* consists of \mathbf{x} and $\boldsymbol{\sigma}$. All previous equations in this section 2.5 can have \mathbf{x} replaced with \mathbf{x}^* to reflect that $\boldsymbol{\sigma}$ are included in the set of parameters evaluated. These extra parameters $\boldsymbol{\sigma}$ are commonly described as "nuisance parameters". These are internal parameters of the statistical analysis that have been introduced to fully compute the likelihood.

2.5.2. Prior. The prior, $f_{X^*}(\mathbf{x}^*)$, represents an initial degree of belief for the \mathbf{x}^* parameter vector. The prior describes the probability of \mathbf{x}^* before any of the currently analyzed data are considered. This function may be a result of engineering intuition or previously collected and analyzed data. Regardless, the prior represents any previous belief in the nature of \mathbf{x}^* and may be overcome with a substantial amount of data to the contrary.

In this study, a uniform prior is used for all model parameters, which gives no preference to any tested values. Jeffrey's prior is used for the nuisance parameters, which gives preference to smaller values of the nuisance parameter,⁴⁷ all with prior independence.

$$f_{X^*}(\mathbf{x}^*) \propto \prod_{z=1}^{n_e} \frac{1}{\sigma_z} \quad (16)$$

This prior provides a basic uninformative model of our prior ignorance, meaning that all tested parameter combinations initially shared equal probability.

2.5.3. Posterior. As previously noted, the posterior, $f_{X^*|Y}(\mathbf{x}^*|\mathbf{y})$, is our desired result as it contains the PDF of the model (and nuisance) parameters, which will provide us with the final calibrated parameters as well as the credible intervals of the parameters. Like the prior, the posterior is a function with $n_p + n_e$ dimensions, where n_p is the number of model parameters for the given soot consumption model. The posterior may be integrated over all parameters except a single desired parameter to obtain the marginal PDF for that parameter. The mode of this marginal PDF is then taken as the calibrated model parameter, and the credible interval is related to the width of the marginal PDF, as detailed below.

The posterior is computed by inserting the prior of eq 16 with the likelihood of eqs 14 and 15 into eq 13 on the right-hand side to give:

$$f_{X^*|Y}(\mathbf{x}^*|\mathbf{y}) \propto \prod_{z=1}^{n_e} \sigma_z^{-(n_{z,i}+1)} \exp\left(-\frac{1}{2\sigma_z^2} \sum_{i=1}^{n_{z,i}} (y_{z,i} - \mu_{z,i}(\mathbf{x}))^2\right) \quad (17)$$

where the $1/\sqrt{2\pi}$ factors have been subsumed into the proportionality constant. To obtain the posterior for only the model parameters of interest, one need only integrate over the nuisance parameters. By identifying that each factor in this product is a function of only one nuisance parameter, we recognized that an implementation will greatly benefit by performing the integrals in a nested hierarchy. This procedure is illustrated mathematically as

$$\begin{aligned} f_{X|Y}(\mathbf{x}|\mathbf{y}) &= \iint \dots \int f_{X^*|Y}(\mathbf{x}^*|\mathbf{y}) d\sigma_1 d\sigma_2 \dots d\sigma_{n_e} \\ &\propto \int \sigma_1^{-(n_{1,i}+1)} \exp\left(-\frac{1}{2\sigma_1^2} \sum_{i=z}^{n_1} (y_{1,i} - \mu_{1,i}(\mathbf{x}))^2\right) d\sigma_1 \times \\ &\quad \int \sigma_2^{-(n_{2,i}+1)} \exp\left(-\frac{1}{2\sigma_2^2} \sum_{i=1}^{n_{2,i}} (y_{2,i} - \mu_{2,i}(\mathbf{x}))^2\right) d\sigma_2 \times \\ &\quad \dots \int \sigma_{n_e}^{-(n_{n_e,i}+1)} \exp\left(-\frac{1}{2\sigma_{n_e}^2} \sum_{i=1}^{n_{n_e,i}} (y_{n_e,i} - \mu_{n_e,i}(\mathbf{x}))^2\right) d\sigma_{n_e} \end{aligned} \quad (18)$$

In this way, the posterior of the parameters of interest can be calculated in a numerical implementation that maintains a low dimensionality. Specifically, the dimensionality at each stage of calculation is the number of model parameters plus one (for the single σ_z corresponding to the current experiment). Then one simply cycles through the experiments. It should be noted that this procedure should not be used at intermediate stages to obtain posteriors for the nuisance parameters.

2.5.4. Implementation. In this study, Bayes' law is used to determine the probability of a set of parameters describing the oxidation and gasification models based on the collected data. Here, an example is detailed showing the steps taken to calibrate parameters in the H_2O portion of the gasification model found in eq 12. A straightforward approach to solution of eq 18 is used. Each experiment is considered sequentially as the multiplicative terms in eq 18 are sequentially evaluated. As noted above, the effective dimensionality of the system needed for evaluation is $n_p + 1$. We discretize the domain of $f_{X|Y}(\mathbf{x}|\mathbf{y})$ using a structured $(n_p + 1)$ -dimensional grid stored as an $(n_p + 1)$ -dimensional array.

1. The parameter values in each dimension were initially determined over a very broad range within the physically possible space. This range was refined to smaller ranges with multiple iterations of these steps to where there was some detectable probability in order to better detail the posterior presented in this work. The gasification by H_2O , eq 12, contains $n_p = 3$ adjustable parameters: $A_{\text{H}_2\text{O}}$, n , and $E_{\text{H}_2\text{O}}$. The final

ranges over which these and all other parameters were tested are shown in Table 3.

Table 3. Range over Which Model Parameters Were Tested

equation	parameter	range
3	A_{O_2}	10^{-2} to 10^2
	E_{O_2}	10^5 to $10^{5.4}$
	A_{OH}	$10^{-3.5}$ to 10^{-2}
11	A_{CO_2}	10^{-18} to 10^{-15}
	E_{CO_2}	0 to 3×10^4
12	A_{H_2O}	10^2 to $10^{7.5}$
	E_{H_2O}	10^5 to 5×10^5
	n	0 to 1

2. The selected ranges are discretized into a series of potential parameter values to be tested in different combinations; 150 points were used for all parameters. Logarithmic spacing was used for all parameters except E_{CO_2} , E_{H_2O} , and n , which had linear spacing.

3. A prior needs to be established. In this study, a uniform prior was used for the model parameters, meaning that all combinations of parameters had uniform probability. Jeffrey's prior was used for the σ_z values. The uniform prior for the model parameters was subsumed in the posterior's normalization constant and not explicitly considered.

4. For the current experiment, at a given point in the $(n_p + 1)$ -dimensional grid (corresponding to a given value of \mathbf{x}^*) modeled rates are computed for each experimental data point. A combination of parameters is selected to be tested against every data point. From these parameters and in computing the modeled rates, the secondary data collected from literature (partial pressures and temperature) are used that correspond to each experimental data point. For H_2O gasification, the modeled rates are computed using eq 12.

5. These modeled rates are compared to the rates given by the data using eq 15 to calculate a likelihood that this combination of

parameters describes a data point. For a given grid point (a given value of \mathbf{x}^*), the likelihood for all points in a given experiment is the product of the likelihoods for the individual data points.

6. This likelihood value is multiplied by the Jeffrey's prior for the σ_z and the uniform prior (done implicitly) for the rate model parameters. The product is a posterior value at the given grid point \mathbf{x}^* for the given experiment.

7. The previous three steps are repeated for each point in the $(n_p + 1)$ -dimensional grid. The result for H_2O gasification is a four dimensional array holding the (unnormalized) posterior PDF for the given experiment, that is, one of the four dimensional product terms z in eq 17.

8. This posterior is then marginalized to remove the σ_z dimension by numerically integrating over all points that shared the same Arrhenius pre-exponential factor, activation energy, and reaction order. That is, by integrating along grid lines in the σ_z direction. This step is portrayed mathematically in eq 18. The resultant three-dimensional unnormalized PDF is the discretized posterior. This posterior can be easily normalized to yield a true PDF so that its (numerical) integral is one.^{45,46}

9. Steps 4–8 are now repeated for the second (and subsequent) experimental data sets. The final posterior, $f_{XY}(\mathbf{x}|y)$, is then the product of the posterior terms for the individual experiments (the integral factors in eq 18). Equivalently, the posterior from step 8 for the previous experiment can be used as the prior of the model parameters for the current experiment since the likelihood is multiplied by the prior in step 6. In this case, a final multiplication of the posterior terms for the individual experiments is not needed since the product is built up sequentially. This interpretation is consistent with the Bayesian approach of making use of prior information as it becomes available. The order in which the experiments are processed does not affect the final posterior, nor does it matter if all the data in the experiments are evaluated in one step or several, as long as each data point is only evaluated once.

10. A final one-dimensional PDF for each individual parameter is produced by marginalizing the multidimensional PDF to each parameter. This is done similarly to the marginalization in step 8 above. For a given single parameter of interest (PoI), the $(n_p - 1)$ -

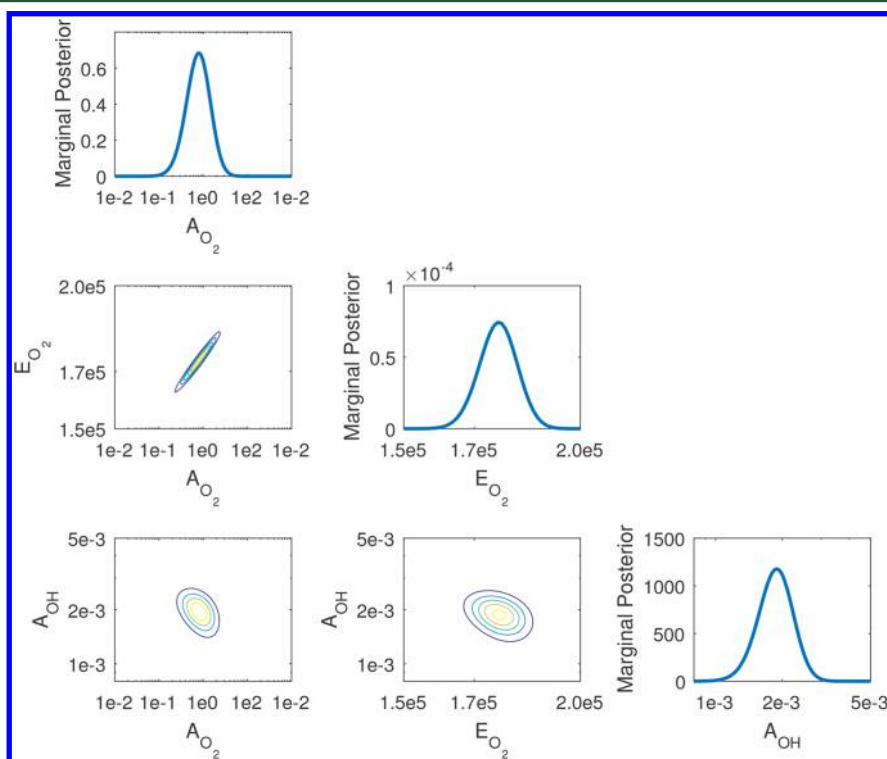


Figure 1. PDFs of each of the oxidation parameters in eq 3. Contours indicate joint PDFs.

dimensional grid at each value of the discrete PoI is numerically integrated, and the result is normalized so that the PDF integrates to one. For H_2O gasification, with $E_{\text{H}_2\text{O}}$ as the PoI, we have the numerical equivalent of

$$f_{E_{\text{H}_2\text{O}}|Y}(E_{\text{H}_2\text{O}}|y) = \iint f_{X|Y}(\mathbf{x}|y) dA_{\text{H}_2\text{O}} d\mathbf{n} \quad (19)$$

3. RESULTS

This section contains results of the Bayesian analysis as applied to the aforementioned data sets. It is important to note that these results are not to be considered absolute but, due to the nature of Bayesian statistics, can and should be updated as more experimental data become available. This is especially important for soot gasification where few data are currently available in the literature.

3.1. Oxidation Model. Results for the parameter calibration of eq 3 can be seen in Figure 1. The three diagonal figures are the resultant marginal PDFs of each of the adjustable parameters. Each PDF is approximately log-normal in appearance. It is interesting to note that the curve for A_{O_2} is much more broad than A_{OH} : the marginal PDF of A_{O_2} spans over 2 full orders of magnitude, while that for A_{OH} spans less than 1 order of magnitude. This is due to the relative importance of these two parameters and the influence of slight variations on the overall rate. In the flame experiments, oxidation by OH is the predominant mechanism of oxidation and tends to influence overall rates more than oxidation by O_2 . As a result, the flame experiments defined A_{OH} , the OH Arrhenius constant, more distinctly than A_{O_2} . E_{O_2} has a sharp peak compared to either A_{O_2} or A_{OH} . This peak is due to the TGA experiments, which were dominated by O_2 oxidation. Slight variations in E_{O_2} had a stronger impact on overall rate than A_{O_2} , the O_2 Arrhenius constant, variations and was therefore more defined. The mode of each of the marginal PDFs is reported in Table 4 as the calibrated parameters for eq

Table 4. Calibrated Parameters for Soot Oxidation, Eq 3

variable	value	90% credible interval		units
		lower bound	upper bound	
A_{O_2}	7.98×10^{-1}	1.94×10^{-1}	5.15	$\frac{\text{kg K}^{1/2}}{\text{Pa m}^2 \text{ s}}$
E_{O_2}	1.77×10^5	1.57×10^5	1.94×10^5	$\frac{\text{J}}{\text{mol}}$
A_{OH}	1.89×10^{-3}	1.06×10^{-3}	3.14×10^{-3}	$\frac{\text{kg K}^{1/2}}{\text{Pa m}^2 \text{ s}}$

3; credible intervals are also shown. The value of $A_{\text{OH}} = 1.89 \times 10^{-3} \frac{\text{kg K}^{1/2}}{\text{Pa m}^2 \text{ s}}$ corresponds to a collision efficiency of 0.15, which is consistent with previous literature values (see ref 18 for a discussion).

The off-diagonal plots of Figure 1 are contour plots showing the relation between the three different parameters. The top of these three plots shows a heavy correlation between A_{O_2} and E_{O_2} . A correlation is to be expected because these two parameters are used in combination to describe the oxidation reaction as occurs by the O_2 molecule. There is a positive correlation between E_{O_2} and A_{O_2} , which is consistent with an increase in A_{O_2} being offset by an increase in E_{O_2} for a given

rate. The shape of the correlation is consistent with the model form. In contrast to the $E_{\text{O}_2}/A_{\text{O}_2}$ PDF, the $A_{\text{OH}}/A_{\text{O}_2}$ and $A_{\text{OH}}/E_{\text{O}_2}$ PDFs show little correlation between their respective parameter pairs. The correlation that is present is slightly negative so that increases in A_{O_2} and E_{O_2} result in decreases in A_{OH} . These low correlations are due to the nature of the experiments from which data was derived. Oxidation in TGA experiments was due entirely to the O_2 mechanism, whereas oxidation in flame experiments was dominated by the OH mechanism.

Figure 2 shows the agreement between rate data collected from the literature and the rates predicted by the calibrated

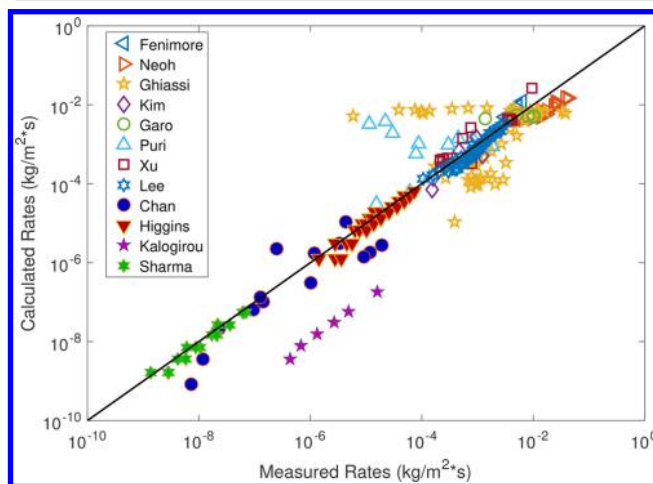


Figure 2. Comparison of predicted rates of soot oxidation by calibrated, with parameters in Table 4, model and those rates collected from the literature. Those experiments that measured only oxidation by O_2 , such as TGA, are filled symbols ($R^2 = 0.75$).

model for soot oxidation by O_2 and OH. This figure displays a parity plot of model calculated rates and literature reported rates. The solid line indicates perfect agreement between the model and the data, so the degree of scatter about this line is a measure of the error in the model and scatter in the measured data. The R^2 statistic (coefficient of determination), using \log_{10}

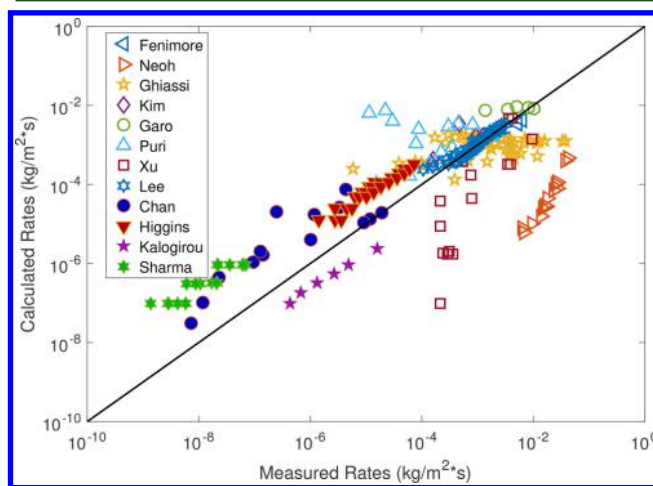


Figure 3. Comparison of oxidation rates as predicted by the NSC oxidation model⁴⁸ and those rates collected from the literature ($R^2 = 0.65$).

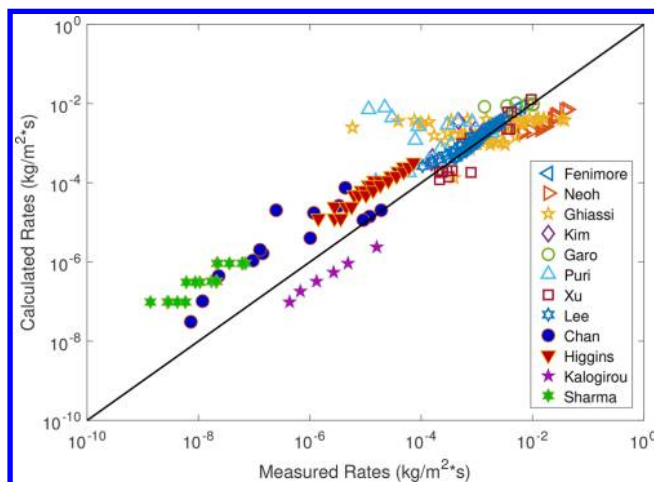


Figure 4. Comparison of oxidation rates as predicted by the NSC oxidation model combined with Neoh et al.³⁰ calculated collision efficiency for OH and those rates collected from the literature ($R^2 = 0.71$).

rates, is 0.75 for this comparison. As can be seen in the figure, there is reasonable agreement between the data and the model with deviations occurring in only a few data sets. For reference, the data span 8 orders of magnitude.

For comparison, Figure 3 shows another parity plot between the collected rates and the rates predicted by the Nagle/Strickland-Constable (NSC) model.⁴⁸ Here, $R^2 = 0.65$. The NSC model represents the oxidation of graphite by O_2 . As can be seen in the figure, the NSC model tends to overpredict oxidation of soot particles for TGA experiments and underpredict oxidation for flame experiments where OH is significant, indicating a significant difference between soot

and graphite surface chemistries. Another common model uses a combination of the NSC O_2 and Neoh OH oxidation models (using a collision efficiency of 0.13, as found by Neoh et al.³⁰). Figure 4 shows the agreement between the collected data and data predicted by this combined model. Here, $R^2 = 0.71$. While this combined model does better than the NSC model alone at predicting soot oxidation, the calibrated model is slightly more accurate (R^2 value of 0.75 vs 0.71). The improvement is modest, however, and indicates that the NSC/Neoh combined model is nearly optimal over a wide range of reported oxidation rates. This is an unexpected but important result.

While it is not the authors' expectation that the proposed model replace the well-established NSC/Neoh combined model on the basis of our results, the use of Bayesian statistics for calibration allows for the quantification of parameter uncertainty as shown in Figure 1, which is not available for parameters in the NSC/Neoh model. The similarity between the NSC/Neoh and the calibrated oxidation models lends confidence to our application of Bayesian statistics to the calibration of the soot gasification models, for which there are no strongly established models in the literature.

3.2. Gasification Model. **3.2.1. H_2O Gasification.** Results for the parameter calibration of H_2O gasification are presented in Figure 5 and Table 5. As in the above discussion, this figure

Table 5. Calibrated Parameters for H_2O Gasification of Soot, Eq 12

variable	value	90% credible interval		Units
		lower bound	upper bound	
A_{H_2O}	6.27×10^4	8.31×10^3	2.47×10^7	$\frac{\text{kg K}^{1/2}}{\text{Pa}^n \text{ m}^2 \text{ s}}$
E_{H_2O}	2.95×10^5	2.66×10^5	3.26×10^5	$\frac{\text{J}}{\text{mol}}$
n	0.13	0.02	0.46	

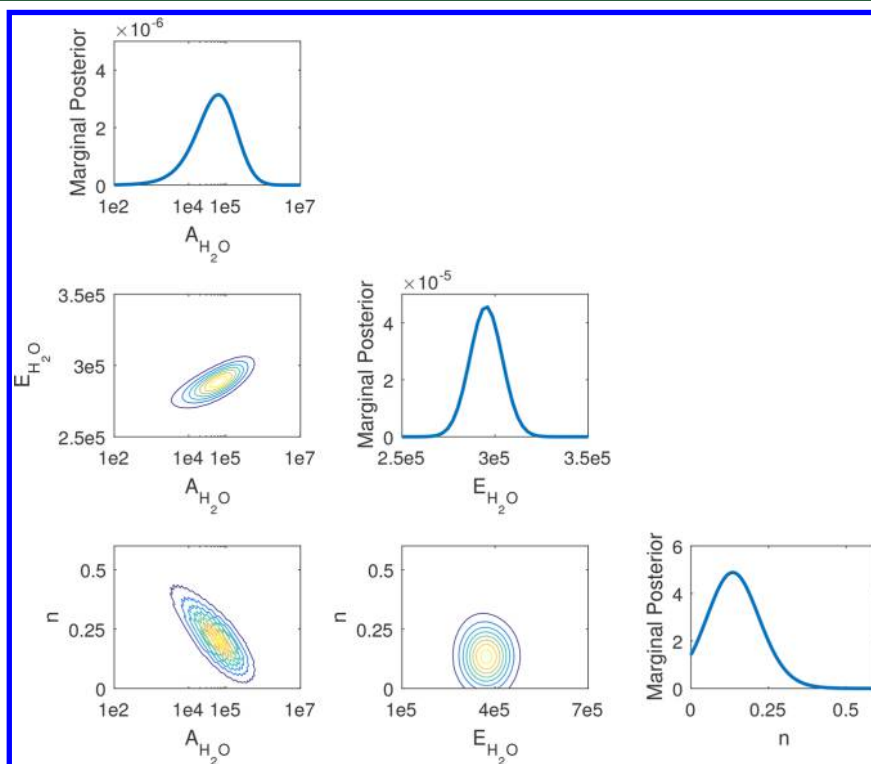


Figure 5. PDFs of each of the H_2O gasification parameters in eq 12.

contains the parameter marginal PDFs on the diagonal plots and contour plots showing the relation between parameters on the off-diagonal plots. Modes of the marginal PDFs are given in Table 5. As expected, the marginal PDFs show fairly clear distributions that could be characterized as approximately log-normal (normal for n). The PDF for the reaction order was only taken out to zero because a negative reaction order was not considered in the form of this global model.

There exists an almost linear correlation between $E_{\text{H}_2\text{O}}$ and the log of $A_{\text{H}_2\text{O}}$, indicating a close linking between these two parameters, as was noted for the oxidation reaction above. However, there is a much different correlation between the reaction order n and either $E_{\text{H}_2\text{O}}$ or $A_{\text{H}_2\text{O}}$, with nearly round contours until the reaction order n drops to low levels. This shape of contour implies that the H_2O reaction order is fairly independent of the other two parameters, except at low values of n , where there appears to be a positive correlation between n and $E_{\text{H}_2\text{O}}$ or $A_{\text{H}_2\text{O}}$. This indicates that the rates are mostly governed by $A_{\text{H}_2\text{O}}$ and $E_{\text{H}_2\text{O}}$, unless the reaction order is sufficiently low (on the order of 0.5 or less), where the other parameters must be adjusted to compensate. Figure 6 shows the

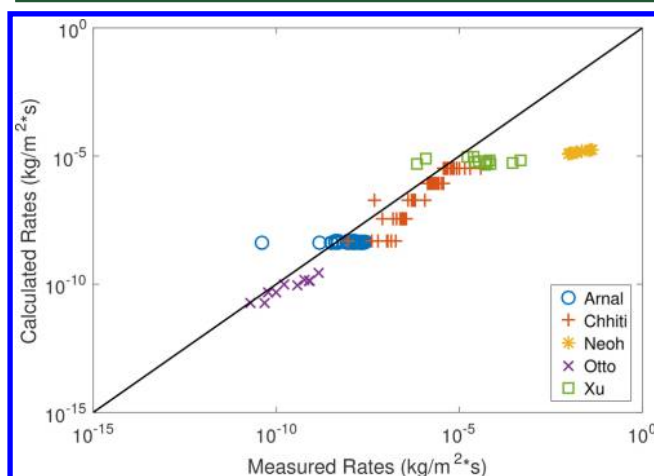


Figure 6. Comparison of predicted rates of soot gasification via H_2O by calibrated model, parameters in Table 5, and those rates collected from the literature ($R^2 = 0.87$ minus Neoh data).

agreement between data collected from the literature and calibrated model prediction using a parity plot like that shown in the previous section. The rate data measured and predicted span 10 orders of magnitude. The agreement between the calibrated model and the data is relatively good, with most predictions within an order of magnitude of the data. Note that individual data sets show consistent bias with respect to the model. For example, the model tends to consistently over-predict the Chhiti data. Considering only a single data set normally would allow better agreement than when considering all sets together.

3.2.2. CO_2 Gasification. Results for the parameter calibration of CO_2 gasification are shown in Figure 7. The two diagonal plots are the marginal PDFs for the two adjustable parameters in eq 11. The modes of these two PDFs are given in the Table 6. The PDF for the activation energy was cut off at zero, and negative activation energies were not considered. The PDF value at an E_{CO_2} value of 0 implies that a straight A_{CO_2} with no exponential activation energy term,

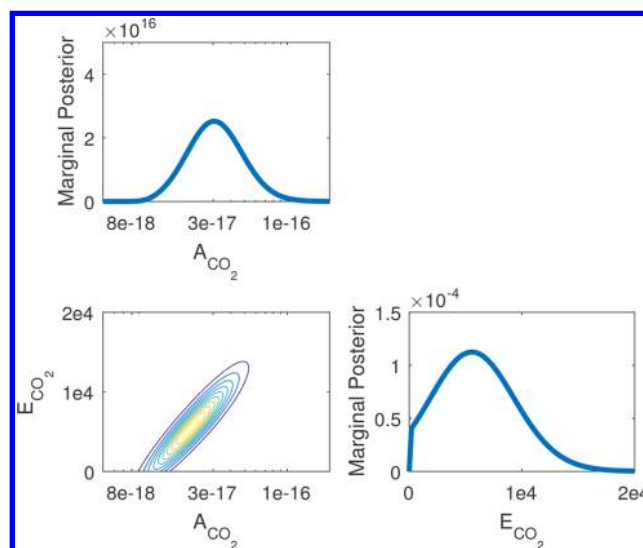


Figure 7. PDFs of each of the CO_2 gasification parameters in eq 11.

Table 6. Calibrated Parameters for CO_2 Gasification of Soot, Eq 11

variable	value	90% credible interval		units
		lower bound	upper bound	
A_{CO_2}	3.06×10^{-17}	1.17×10^{-17}	1.57×10^{-16}	$\frac{\text{kg}}{\text{Pa}^{1/2} \text{K}^2 \text{m}^2 \text{s}}$
E_{CO_2}	5.56×10^3	6.04×10^2	1.95×10^4	$\frac{\text{J}}{\text{mol}}$

$$r_{\text{CO}_2} = A_{\text{CO}_2} P_{\text{CO}_2}^{0.5} T^2 \quad (20)$$

could be used to describe the data, but not as well as the current proposed model. The authors expect that more data would support the form of this model and the activation energy PDF would become more narrow within the positive range. The full PDF of these parameters is shown in the contour plot in Figure 7. As can be seen in this plot, E_{CO_2} and the log of A_{CO_2} are highly correlated in a linear relationship, as expected by the model form.

Figure 8 shows the parity plot of the data and the calibrated model for the CO_2 gasification rates. A large amount of scatter is seen in this plot and the model is much less accurate than for the oxidation and H_2O gasification rates. This discrepancy is due to the combined effects of inconsistencies between experiments and the inability of the model form chosen to reproduce these data sets as accurately. The data in the four sets span approximately 4 orders of magnitude. The model captures the measured rates within an order of magnitude for most of the data points.

Figure 9 shows the same parity plots as above, but here the gasification model has been individually calibrated to each data set instead of all the data sets combined. As can be seen in the figure, the proposed model fits three of the four data sets, with some difficulty in fitting the data measured by Kajitani et al.²⁶ This indicates that the form of the model used was reasonable but there may be differences between data sets that could be explored more thoroughly.

Gasification rates tend to be much smaller than oxidation rates, small enough that simple thermal pyrolysis of soot samples may not be considered negligible in these experiments. As a result, some of the experiments may appear to gasify faster than others due to differences in pyrolysis. In addition, the

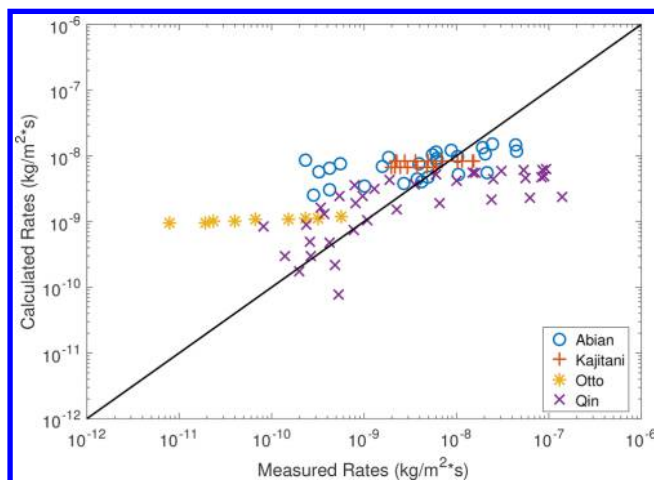


Figure 8. Comparison of predicted rates of soot gasification via CO_2 by calibrated model, parameters from Table 6, and those rates collected from the literature ($R^2 = 0.62$).

structure of the soot particle surface may have a much larger impact on gasification than on oxidation. Two of these experiments were carried out with the expressed purpose of exploring changes in the rate as the surface chemistry changed over time.^{16,26} The model used here does not account for such changes. Despite these and other factors, the model form chosen was the best of those tested. As more experimentation is carried out and more data become available in the literature, a more accurate model should be compiled and calibrated using the techniques discussed in this study.

3.3. Rate Prediction. The above models can be used to predict soot consumption rates along with a quantified uncertainty for those predictions. This is illustrated in this section using, for instance, the Higgins et al.³⁶ data for soot oxidation.

In Figure 10, a PDF of the rate in eq 3 is shown for a single data point measured by Higgins where the flame has a

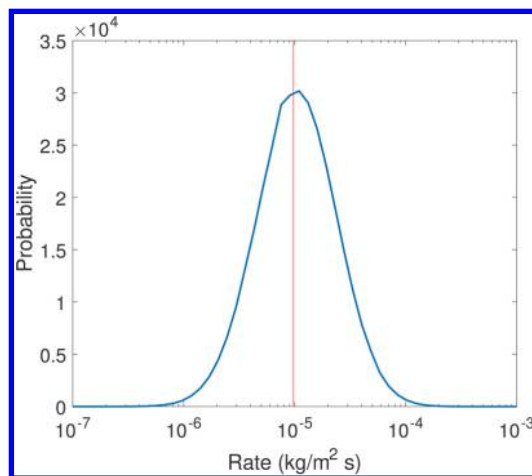


Figure 10. PDF of the calculated gasification rate in Higgins experiment where the flame data was at 1200 K.

temperature of 1225 K and partial pressures of $P_{\text{O}_2} = 21\,300$ Pa and $P_{\text{OH}} = 6.22 \times 10^{-7}$ Pa. This PDF is obtained from the full joint PDF calculated for the oxidation parameters and displayed in Figure 1. Each combination of parameters tested results in a calculated rate; the associated probability with that combination of parameters is equal to the probability of the calculated rate. Just as with the marginal PDFs displayed in Figure 1, a normalization constant is computed and used to determine the final PDF of Figure 10.

The vertical line in the figure indicates the measured rate reported by Higgins and falls near the center of the calculated PDF. This PDF was calculated using discrete bins. The width of the calculated PDF indicates the uncertainty in this calculation. As more data are analyzed from the literature, this PDF will narrow and the uncertainty will shrink.

Figure 11 shows the comparison of multiple data points measured by Higgins compared to the model predicted rates. There were two independent measurements taken out at each

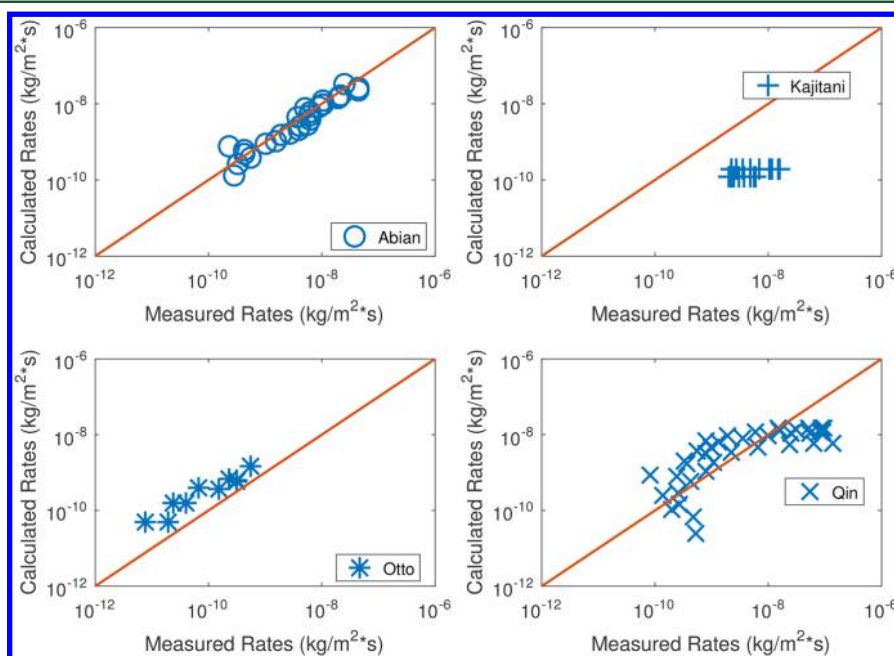


Figure 9. Comparison of predicted rates of soot gasification via CO_2 by individually calibrated models and those rates collected from the literature.

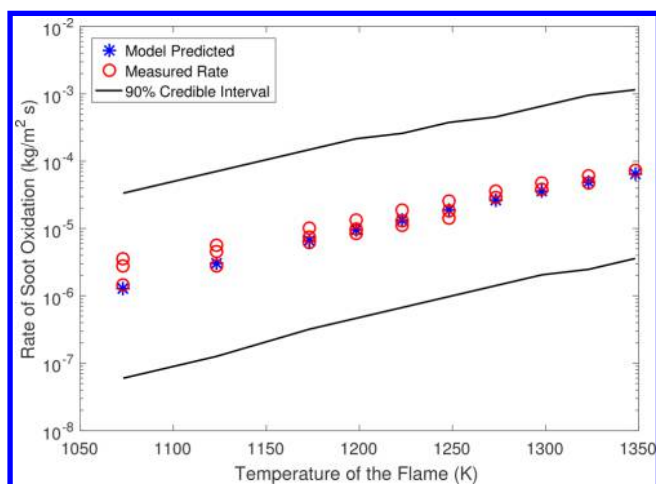


Figure 11. Comparison of the model predicted oxidation rate with confidence bounds versus the measured rate in Higgins's experiment.

temperature by the experimenters, and all measurements are shown in this plot. This figure also shows a 90% credible interval evaluated from the calculated PDF at each point. Like Figure 10, Figure 11 indicates that with the current analysis there is a moderate degree of uncertainty in the oxidation model, but all the reported rates lie close to the center of the calculated uncertainty bounds.

4. DISCUSSION

The previous section demonstrated the use of Bayesian statistics to calibrate global models for soot consumption. This method of model calibration has a few advantages and disadvantages over more traditional model calibration techniques, such as minimization of summed square error.

The first clear advantage of using a Bayesian calibration method, compared to that of a least-summed-squares, is the production of a full PDF for the parameter-space from which uncertainty quantification can be easily extracted. Other methods of extracting uncertainty from calibrated parameters assume a fixed PDF for the parameter space and test from that distribution using either Student's *t* test or an *f*-test.⁴⁹

This full PDF comes at a cost. The computational cost of a full Bayesian analysis scales by a power equal to the number of parameters used in the models plus any nuisance parameters. In the case of the soot consumption model calibrated in this study, when the parameter space of the oxidation model was doubled the number of computations required was increased 16-fold. There are methods to reduce the computational costs of a Bayesian analysis such as the use of Markov chain Monte Carlo (MCMC) methods. MCMC methods are a class of algorithms for sampling from the probability space based on the use of a Markov chain that evolves a posterior distribution through sampling until an equilibrium is obtained. These algorithms are an intense field of research, and results have become very robust and hold much promise for parameter calibration in simple and complex models.^{50,51} Even with such improvements, least-summed-squares usually requires only a fraction of the computation cost. However, for the present study, computational costs did not limit the technique.

In principle, the final result of a least-summed-squares calibration and a Bayesian calibration should yield the same results.⁴⁵ Both methods are based the use of the Gaussian Distribution found in eq 15. Because σ is a nuisance parameter,

to maximize the probability of this distribution, the numerator of the exponential should be minimized:

$$\max(p(y_{z,i} | \mu_z(\mathbf{x}), \sigma_z)) = \min((y_{z,i} - \mu_z(\mathbf{x}))^2) \quad (21)$$

which is the basis of least-summed-squares.

In the case of Bayesian calibration, this distribution is used as the likelihood function. Once the probability space is calculated, the mode is used as the calibrated parameter set. In this study, the modes of the marginal parameter PDFs were used instead of the absolute mode of the probability space, but these tend to be the same for simple, single-peaked topologies, as occur in Figures 1, 5, and 7. If the probability surface topology is more complex, for example, with multiple peaks of high probability, the mode of the probability space will differ from the mode of the parameter-marginal PDFs. This is an indication that there is likely disagreement between data sets and the proposed model and is clearly indicated by the Bayesian processes, in contrast to a least-squared-sum analysis that would not necessarily reveal this discrepancy.

The Bayesian analysis presented is a calibration technique for parameters of a given model. This analysis is not strictly a model optimization because the form of the model does not change during the analysis, only the parameter values.⁵² In this study, different forms of a soot consumption model were analyzed including a collision-efficiency model, simple Arrhenius equations, and modified Arrhenius equations, with varied temperature and concentration dependencies.

5. CONCLUSIONS

Global models for soot particle oxidation and gasification were presented with parameters calibrated using Bayesian methods. Besides providing the model parameters, this method also gives full joint parameter PDFs and uncertainties, which provide more detailed information, with fewer assumptions, than are available by other methods such as by minimizing least sum square errors. PDFs of the calibration were presented along with parity plots displaying agreement between model predicted rates and those collected from the literature. The oxidation model shows good results and was robust enough for use in large scale simulation. The gasification model showed reasonable results for H₂O gasification, but only marginal results for CO₂ gasification when considering all data sets. Individual data sets could be fit with much more accuracy. The *R*² values for the oxidation and H₂O and CO₂ gasification models are 0.75, 0.87, and 0.62, respectively. As new data become available, these could easily be incorporated into the model to reduce uncertainty in the calibrated model parameters. This is especially true for the performance of the CO₂ gasification. Further research into model forms including additional soot physics could reduce possible model bias and possibly improve consistency among experiments. While the oxidation model was an improvement over the NSC O₂ + Neoh OH combined oxidation model *R*² = 0.71, the improvement is modest.

The calibrated oxidation model can be used to calculate rates along with their uncertainties. An example was given using the Higgins et al.³⁶ experiments. Results were compared to the data, and it was found that all reported data fell within determined credible intervals of the model.

■ ASSOCIATED CONTENT

● Supporting Information

The Supporting Information is available free of charge on the ACS Publications website at DOI: 10.1021/acs.energyfuels.7b00899.

Raw and derived soot oxidation and CO₂, H₂O gasification data from the cited literature sources (XLSX)

Matlab code used for Bayesian parameter calibration analysis, file 1 of 3, file tutorial.m (TXT)

Matlab code used for Bayesian parameter calibration analysis, file 2 of 3, file bayesian.m (TXT)

Matlab code used for Bayesian parameter calibration analysis, file 3 of 3, file quadratic_model.m (TXT)

■ AUTHOR INFORMATION

Corresponding Author

*E-mail: davidlignell@byu.edu.

ORCID

Thomas H. Fletcher: 0000-0002-9999-4492

David O. Lignell: 0000-0002-2129-1375

Notes

The authors declare no competing financial interest.

Matlab code and raw data are also available at <https://github.com/sootconsumption/Soot-Consumption-Modeling-with-Bayesian-Statistics>.

■ ACKNOWLEDGMENTS

The work was supported by the Department of Energy, National Nuclear Security Administration, under Award DE-NA0002375.

■ NOMENCLATURE

A_{CO_2} = Arrhenius pre-exponential factor for CO₂ gasification, $\frac{\text{kg}}{\text{Pa}^{1/2} \text{K}^2 \text{m}^2 \text{s}}$, eqs 11, 20

$A_{\text{H}_2\text{O}}$ = Arrhenius pre-exponential factor for H₂O gasification, $\frac{\text{kg K}^{1/2}}{\text{Pa}^n \text{m}^2 \text{s}}$, eq 12

A_{O_2} = Arrhenius pre-exponential factor for O₂ oxidation, $\frac{\text{kg K}^{1/2}}{\text{Pa m}^2 \text{s}}$, eq 3

A_{OH} = Arrhenius pre-exponential factor for OH oxidation, $\frac{\text{kg K}^{1/2}}{\text{Pa m}^2 \text{s}}$, eq 3

C_i = molar concentration of species i , $\frac{\text{mol}}{\text{m}^3}$, eq 4

d_1 = initial particle diameter, m, eqs 5, 7

d_2 = particle diameter after oxidation, m, eq 5

E_i = activation energy for species i consumption, $\frac{\text{J}}{\text{mol}}$, eqs 3, 11, 12

k = Arrhenius rate constant, $\frac{1}{\text{s}}$, eq 6

$m_{\text{cr},i}$ = mass of carbon removed from soot surface, $\frac{\text{kg}}{\text{mol}}$, eq 4

n = species reaction order in the rate equation, unitless, eqs 6, 12

n_e = number of experiments, unitless, eqs 14, 16, 18

n_p = number of parameters for a given soot model, unitless

$n_{z,i}$ = number of data points in experiment z , unitless, eqs 14, 17

X_{O_2} = mole fraction of O₂ in the gas phase, unitless, eq 6

P_i = partial pressure of species i , Pa, eq 3, 11, 12

R = ideal gas constant, $\frac{\text{J}}{\text{mol K}}$, eqs 3, 11, 12, 20

r_{CO_2} = gasification rate due to CO₂, $\frac{\text{kg}}{\text{m}^2 \text{s}}$, eq 10, 11, 20

r_{gs} = gasification rate, $\frac{\text{kg}}{\text{m}^2 \text{s}}$, eq 10

$r_{\text{H}_2\text{O}}$ = gasification rate due to H₂O, $\frac{\text{kg}}{\text{m}^2 \text{s}}$, eqs 10, 12

r_{ox} = oxidation rate, $\frac{\text{kg}}{\text{m}^2 \text{s}}$, eqs 3, 4, 5, 7

$r_{\text{ox,rep}}$ = reported oxidation rate, s⁻¹, eq 7

T = local temperature, K, eqs 3, 11, 12, 20

t = residence time, s, eq 5

\bar{v} = Boltzmann equilibrium mean molecular velocity, $\frac{\text{m}}{\text{s}}$, eq 4

\mathbf{x} = vector of model parameters, various units, eqs 14, 15, 17, 18, 21

\mathbf{x}^* = vector of all parameters (with nuisance parameters), various units, eqs 13, 14, 16, 17, 18

\mathbf{y} = vector of experimental data, $\frac{\text{kg}}{\text{m}^2 \text{s}}$, eqs 13, 14, 17, 18

$y_{z,i}$ = single experimental data point, $\frac{\text{kg}}{\text{m}^2 \text{s}}$, eqs 14, 15, 17, 18, 21

η_i = Species collision efficiency, unitless, eq 4

μ_z = model prediction, $\frac{\text{kg}}{\text{m}^2 \text{s}}$, eqs 14, 15, 17, 18, 21

ρ_s = soot density, $\frac{\text{kg}}{\text{m}^3}$, eqs 5, 7

$\boldsymbol{\sigma}$ = vector of standard deviations, $\frac{\text{kg}}{\text{m}^2 \text{s}}$

σ_z = standard deviation (nuisance parameter), $\frac{\text{kg}}{\text{m}^2 \text{s}}$, eqs 14, 15, 16, 17, 18, 21

■ REFERENCES

- (1) Kennedy, I. M. The health effects of combustion-generated aerosols. *Proc. Combust. Inst.* **2007**, *31*, 2757–2770.
- (2) U.S. Department of Energy, Annual Energy Review 2006, DOE/EIA-0384 2006, URL: <http://www.eia.doe.gov/emeu/aer/contents.html>, Posted June 27, 2007.
- (3) Gorbunov, B.; Baklanov, A.; Kakutkina, N.; Windsor, H. L.; Toumi, R. Ice nucleation on soot particles. *J. Aerosol Sci.* **2001**, *32*, 199–215.
- (4) O'Driscoll, C. Climate change soot warming significant. *Chem. Ind.* **2011**, *75* (17), 10.
- (5) Viskanta, R.; Menguc, M. P. Radiation heat-transfer in combustion systems. *Prog. Energy Combust. Sci.* **1987**, *13*, 97–160.
- (6) Bockhorn, H. *Soot formation in combustion: mechanisms and models*; Springer series in chemical physics; Springer-Verlag: Berlin; New York, 1994.
- (7) Bockhorn, H.; D'Anna, A.; Sarofim, A.; Wang, H., Eds. *Combustion Generated Fine Carbonaceous Particles*; KIT Scientific Publishing, 2009.
- (8) Neoh, K. G. Soot burnout in flames. Ph.D. thesis, Massachusetts Institute of Technology, 1981.
- (9) Lee, K. B.; Thring, M. W.; Beer, J. M. On the rate of combustion of soot in a laminar soot flame. *Combust. Flame* **1962**, *6*, 137–145.
- (10) Stanmore, B. R.; Brilhac, J. F.; Gilot, P. The oxidation of soot: a review of experiments, mechanisms and models. *Carbon* **2001**, *39*, 2247–2268.
- (11) Lighty, J. S.; Romano, V.; Sarofim, A. F. In *Combustion Generated Fine Carbonaceous Particles*; Bockhorn, H., D'Anna, A., Sarofim, A. F., Wang, H., Eds.; KIT Scientific Publishing, 2009; p 754.
- (12) Vierbaum, R.; Roth, P. High-temperature oxidation of dispersed soot particles by O atoms. *Proc. Combust. Inst.* **2002**, *29*, 2423–2429.
- (13) Toftegaard, M. B.; Brix, J.; Jensen, P. A.; Glarborg, P.; Jensen, A. D. Oxy-fuel combustion of solid fuels. *Prog. Energy Combust. Sci.* **2010**, *36*, 581–625.

- (14) Buhre, B. J. P.; Elliott, L. K.; Sheng, C. D.; Gupta, R. P.; Wall, T. F. Oxy-fuel combustion technology for coal-fired power generation. *Prog. Energy Combust. Sci.* **2005**, *31*, 283–307.
- (15) Fletcher, T. H.; Ma, J. L.; Rigby, J. R.; Brown, A. L.; Webb, B. W. Soot in coal combustion systems. *Prog. Energy Combust. Sci.* **1997**, *23*, 283–301.
- (16) Abian, M.; Jensen, A. D.; Glarborg, P.; Alzueta, M. U. Soot reactivity in conventional combustion and oxy-fuel combustion environments. *Energy Fuels* **2012**, *26*, 5337–5344.
- (17) Ghiassi, H.; Jaramillo, I. C.; Lighty, J. S. Kinetics of soot oxidation by molecular oxygen in a premixed flame. *Energy Fuels* **2016**, *30*, 3463–3472.
- (18) Ghiassi, H.; Lignell, D.; Lighty, J. S. Soot oxidation by OH: theory development, model, and experimental validation. *Energy Fuels* **2017**, *31*, 2236–2245.
- (19) Sirignano, M.; Ghiassi, H.; D'Anna, A.; Lighty, J. S. Temperature and oxygen effects on oxidation-induced fragmentation of soot particles. *Combust. Flame* **2016**, *171*, 15–26.
- (20) Qin, K.; Lin, W. G.; Faester, S.; Jensen, P. A.; Wu, H.; Jensen, A. D. Characterization of residual particulates from biomass entrained flow gasification. *Energy Fuels* **2013**, *27*, 262–270.
- (21) Trubetskaya, A.; Jensen, P. A.; Jensen, A. D.; Llamas, A. D. G.; Umeki, K.; Gardini, D.; Kling, J.; Bates, R. B.; Glarborg, P. Effects of several types of biomass fuels on the yield, nanostructure and reactivity of soot from fast pyrolysis at high temperatures. *Appl. Energy* **2016**, *171*, 468–482.
- (22) Garo, A.; Prado, G.; Lahaye, J. Chemical aspects of soot particles oxidation in a laminar methane - air diffusion flame. *Combust. Flame* **1990**, *79*, 226–233.
- (23) Shurtz, R. C.; Fletcher, T. H. Coal char-CO₂ gasification measurements and modeling in a pressurized flat-flame burner. *Energy Fuels* **2013**, *27*, 3022–3028.
- (24) Ghiassi, P.; Jaramillo, I. C.; Toth, P.; Lighty, J. Soot oxidation-induced fragmentation: Part 1: The relationship between soot nanostructure and oxidation-induced fragmentation. *Combust. Flame* **2016**, *163*, 179–187.
- (25) Ghiassi, H.; Jaramillo, I.; Toth, P.; Lighty, J. Soot oxidation-induced fragmentation: Part 2: Experimental investigation of the mechanism of fragmentation. *Combust. Flame* **2016**, *163*, 170–178.
- (26) Kajitani, S.; Zhang, Y.; Umemoto, S.; Ashizawa, M.; Hara, S. Co-gasification reactivity of coal and woody biomass in high-temperature gasification. *Energy Fuels* **2010**, *24*, 145–151.
- (27) Guo, H.; Anderson, P. M.; Sunderland, P. B. Optimized rate expressions for soot oxidation by OH and O₂. *Fuel* **2016**, *172*, 248–252.
- (28) Kalogirou, M.; Samaras, Z. Soot oxidation kinetics from TG experiments. *J. Therm. Anal. Calorim.* **2010**, *99*, 1005–1010.
- (29) Fenimore, C. P.; Jones, G. W. Oxidation of soot by hydroxyl radicals. *J. Phys. Chem.* **1967**, *71*, 593.
- (30) Neoh, K. G.; Howard, J. B.; Sarofim, A. F. In *Particulate Carbon*; Siegl, D., Smith, G., Eds.; Springer: US, 1981; pp 261–282.
- (31) Kim, C. H.; El-Leathy, A. M.; Xu, F.; Faeth, G. M. Soot surface growth and oxidation in laminar diffusion flames at pressures of 0.1–1.0 atm. *Combust. Flame* **2004**, *136*, 191–207.
- (32) Kim, C. H.; Xu, F.; Faeth, G. M. Soot surface growth and oxidation at pressures up to 8.0 atm in laminar nonpremixed and partially premixed flames. *Combust. Flame* **2008**, *152*, 301–316.
- (33) Puri, R.; Santoro, R. J.; Smyth, K. C. The oxidation of soot and carbon-monoxide in hydrocarbon diffusion flames. *Combust. Flame* **1994**, *97*, 125–144.
- (34) Xu, F.; El-Leathy, A. M.; Kim, C. H.; Faeth, G. M. Soot surface oxidation in hydrocarbon/air diffusion flames at atmospheric pressure. *Combust. Flame* **2003**, *132*, 43–57.
- (35) Chan, M. L.; Moody, K. N.; Mullins, J. R.; Williams, A. Low-temperature oxidation of soot. *Fuel* **1987**, *66*, 1694–1698.
- (36) Higgins, K. J.; Jung, H. J.; Kittelson, D. B.; Roberts, J. T.; Zachariah, M. R. Size-selected nanoparticle chemistry: kinetics of soot oxidation. *J. Phys. Chem. A* **2002**, *106*, 96–103.
- (37) Sharma, H. N.; Pahalagedara, L.; Joshi, A.; Suib, S. L.; Mhadeshwar, A. B. Experimental study of carbon black and diesel engine soot oxidation kinetics using thermogravimetric analysis. *Energy Fuels* **2012**, *26*, 5613–5625.
- (38) Goodwin, D. et al. *Cantera, an object-oriented software toolkit for chemical kinetics, thermodynamics, and transport processes*. <http://www.cantera.org>, 2011.
- (39) Mendiara, T.; Domene, M. P.; Millera, A.; Bilbao, R.; Alzueta, M. U. An experimental study of the soot formed in the pyrolysis of acetylene. *J. Anal. Appl. Pyrolysis* **2005**, *74*, 486–493.
- (40) Christensen, J. M.; Grunwaldt, J. D.; Jensen, A. D. Effect of NO₂ and water on the catalytic oxidation of soot. *Appl. Catal., B* **2017**, *205*, 182–188.
- (41) Hurt, R. H.; Sarofim, A. F.; Longwell, J. P. Gasification-induced densification of carbons - from soot to form coke. *Combust. Flame* **1993**, *95*, 430–432.
- (42) Otto, K.; Sieg, M.; Zinbo, M.; Bartosiewicz, L. The oxidation of soot deposits from diesel engines. *SAE Tech. Pap. Ser.* **1980**, *13*.
- (43) Arnal, C.; Alzueta, M. U.; Millera, A.; Bilbao, R. Influence of water vapor addition on soot oxidation at high temperature. *Energy* **2012**, *43*, 55–63.
- (44) Chhiti, Y.; Peyrot, M.; Salvador, S. Soot formation and oxidation during bio-oil gasification: experiments and modeling. *J. Energy Chem.* **2013**, *22*, 701–709.
- (45) Jaynes, E. T.; Bretthorst, G. L. *Probability theory: the logic of science*; Cambridge University Press: New York, 2003.
- (46) Gelman, A. *Bayesian data analysis*; Chapman & Hall/CRC: Boca Raton, FL, 2004.
- (47) Fevotte, C.; Godsill, S. J. In *Independent Component Analysis and Blind Signal Separation, Proceedings*; Rosca, J., Erdogmus, D., Principe, J. C., Haykin, S., Eds.; Lecture Notes in Computer Science; Springer-Verlag Berlin: Berlin, 2006; Vol. 3889; pp 593–600.
- (48) Nagle, J.; Strickland-Constable, R. F. *Proceedings of the Fifth Conference on Carbon*; Pergamon, 1962; pp 154–164.
- (49) Gilliland, D.; Li, M. A note on confidence intervals for the power of t-test. *Statistics & Probability Letters* **2008**, *78*, 488–489.
- (50) Haario, H.; Saksman, E.; Tamminen, J. An adaptive metropolis algorithm. *Bernoulli* **2001**, *7*, 223–242.
- (51) Haario, H.; Laine, M.; Saksman, E.; Mira, A. DRAM: Efficient adaptive MCMC. *Statistics and Computing* **2006**, *16*, 339–354.
- (52) Jain, A.; Srinivasulu, S. In *Practical Hydroinformatics*; Abraham, R. J., See, L. M., Solomatine, D. P., Eds.; Springer: Berlin Heidelberg, 2008; Chapter IV, pp 291–301.